Superfluid–Mott-insulator quantum phase transition of light in a two-mode cavity array with ultrastrong coupling

Jingtao Fan,[1,2] Yuanwei Zhang,[3] Lirong Wang,[1,2] Feng Mei,[1,2,*] Gang Chen,[1,2,†] and Suotang Jia[1,2]

[1]*State Key Laboratory of Quantum Optics and Quantum Optics Devices, Institute of Laser Spectroscopy, Shanxi University, Taiyuan 030006, China*

[2]*Collaborative Innovation Center of Extreme Optics, Shanxi University, Taiyuan 030006, China*

[3]*College of Physics and Electronic Engineering, Sichuan Normal University, Chengdu 610068, China*

(Received 24 January 2017; published 29 March 2017)

In this paper we construct a type of cavity array, in each cavity of which multiple two-level atoms interact with two independent photon modes. This system can be totally governed by a two-mode Dicke-lattice model, which includes all of the counter-rotating terms and therefore works well in the ultrastrong coupling regime achieved in recent experiments. Attributed to its special atom-photon coupling scheme, this model supports a global conserved excitation and a continuous U(1) symmetry, rather than the discrete Z_2 symmetry in the standard single-mode Dicke-lattice model. This distinct change of symmetry via adding an extra photon mode strongly impacts the nature of photon localization and delocalization behavior. Specifically, the atom-photon interaction features stable Mott-lobe structures of photons and a second-order superfluid–Mott-insulator quantum phase transition, which share similarities with the Jaynes-Cummings-lattice and Bose-Hubbard models. More interestingly, the Mott-lobe structures predicted here depend crucially on the atom number of each site. We also show that our model can be mapped into a continuous XX spin model. Finally, we propose a scheme to implement the introduced cavity array in circuit quantum electrodynamics. This work broadens our understanding of strongly correlated photons.

DOI: 10.1103/PhysRevA.95.033842

I. INTRODUCTION

Photons are excellent information carriers in nature and generally pass through each other without consequence. The realization of coherent manipulation and controlling of photons allows us to achieve photon quantum information processing [1] as well as to explore exotic many-body phenomena of photons [2]. Cavity array [3–7], in which each single-mode cavity interacts with a two-level atom, is a promising platform to accomplish the required target and has now been considered extensively [8–26]. This platform has a novel interplay between strong local nonlinearities and photon hopping of the nearest-neighbor cavities, which has a phenomenological analogy to those of the Bose-Hubbard model [27–31] realized, for example, by ultracold atoms in optical lattices [32]. More importantly, however, compared with condensed-matter or atomic physics, cavity array has the unique property that the fundamental many-body phenomena depend crucially on the intrinsic atom-photon coupling strength [3–7].

For the weak and moderately strong coupling regimes, the counter-rotating terms of the single-site Hamiltonian are usually neglected by employing the rotating-wave approximation. As a result, the property of cavity array is governed by a Jaynes-Cummings-lattice model [3–7]. Since this Jaynes-Cummings-lattice model preserves a global excitation number, a series of Mott-insulator (MI) phases of photons forms a lobe structure, and a second-order superfluid (SF)-MI zero-temperature ($T=0$) quantum phase transition takes place across the edge of each lobe. This Mott-lobe structure makes it a photonic counterpart of the Bose-Hubbard model [27–31], which simulates massive bosons in lattice and also supports a similar lobe structure. However, it should be noticed that a complete description of the light-matter interaction should always incorporate the counter-rotating terms, especially considering the fact that recent experiments of circuit quantum electrodynamics (QED) have accessed the ultrastrong coupling regime (i.e., the atom-photon coupling strength has the same order of the photon frequency) [33–36], in which the rotating-wave approximation totally breaks down. In such a case, a proper description of the system dynamics should resort to a Rabi-lattice model [37–41]. Since the counter-rotating terms in the Rabi-lattice model break the conservation of excitation number, there is, in principle, no similar MI as that of the Bose-Hubbard model, and the transition between the SF and MI should be replaced by the coherent and incoherent types [38,39]. These essential changes of equilibrium properties motivate us to ask a question: Could the Mott-lobe structure still exist even though all of the counter-rotating terms of the atom-photon coupling are taken into consideration?

In the present paper, we try to answer this question by constructing a type of cavity array, in each cavity of which multiple two-level atoms interact with two independent photon modes. This system can be totally governed by a two-mode Dicke-lattice (TMDL) model, which includes all of the counter-rotating terms and therefore works well in the ultrastrong coupling regime. Our focus is the ground-state property of such a system. Unlike the single-mode Rabi-lattice model [37–41], the considered TMDL model has a global conserved excitation and a continuous U(1) symmetry. This distinct change of symmetry via adding an extra photon mode induces some interesting many-body physics of strongly correlated photons. Specifically, the atom-photon interaction features stable Mott-lobe structures of photons and a second-order SF-MI quantum phase transition, which share similarities with the Jaynes-Cummings-lattice [3–7] and Bose-Hubbard [27–31] models. However, in contrast to these models, the Mott-lobe

*raulmei@163.com
†chengang971@163.com

 ©2017 American Physical Society

structures predicted here depend crucially on the atom number of each site, reflecting its particularity among lattice models. We also show that the TMDL model can be mapped into a continuous XX spin model under proper parameter conditions. Finally, motivated by recent experimental achievements of cavity array [42–44] and multimode cavity [45–47] in circuit QED, we propose a scheme to realize the TMDL model in a two-mode superconducting stripline cavity array. This work broadens our understanding of strongly correlated photons.

II. MODEL AND HAMILTONIAN

We study a photon lattice system composed of an array of identical coupled cavities, inside each of which multiple two-level atoms interact with two degenerate photon modes. Such a system is governed by the TMDL Hamiltonian

$$\hat{H}_{\mathrm{T}} = \sum_{j} \hat{H}_{j}^{\mathrm{TD}} - t \sum_{\langle j,k\rangle} \sum_{m=1,2} \hat{a}_{m,j}^{\dagger} \hat{a}_{m,k}, \tag{1}$$

where the single-site Hamiltonian

$$\hat{H}_{j}^{\mathrm{TD}} = \omega \sum_{m=1,2} \hat{a}_{m,j}^{\dagger} \hat{a}_{m,j} + \omega_0 \hat{J}_{z,j} + g[(\hat{a}_{1,j} + \hat{a}_{1,j}^{\dagger})\hat{J}_{x,j} + i(\hat{a}_{2,j} - \hat{a}_{2,j}^{\dagger})\hat{J}_{y,j}]. \tag{2}$$

In Hamiltonians (1) and (2), $\hat{a}_{m,j}^{\dagger}$ and $\hat{a}_{m,j}$ are the creation and annihilation operators of the mth photon mode of site j, $\hat{J}_{i,j}(i = x,y,z) = \sum_{l=1}^{N} \hat{\sigma}_{i,j}^{l}/2$, with $\hat{\sigma}_{i,j}^{l}$ being the Pauli spin operator, is the collective spin operator of site j, ω is the frequency of the degenerate photon modes, ω_0 is the atom resonant frequency, g is the atom-photon coupling strength, t is the hopping rate, and $\langle j,k\rangle$ denotes the photon hopping between the nearest-neighbor sites j and k.

An intriguing feature of Hamiltonian (2) is that the spin operator couples to the two independent photon modes via its two orthogonal components $\hat{J}_x$ and $\hat{J}_y$. It should be noticed that this kind of atom-photon interaction is just the celebrated Jahn-Teller $E \otimes e$ coupling in molecular and condensed-matter physics [48], which has also been systematically studied from the perspectives of cavity QED [49,50] and ion crystals [51]. Without the coupling term $i(\hat{a}_{2,j} - \hat{a}_{2,j}^{\dagger})J_{y,j}$, Hamiltonian (2) reduces to the standard single-mode Dicke model

$$\hat{H}_{j}^{\mathrm{D}} = \omega \hat{a}_{1,j}^{\dagger} \hat{a}_{1,j} + \omega_0 \hat{J}_{z,j} + g(\hat{a}_{1,j} + \hat{a}_{1,j}^{\dagger})\hat{J}_{x,j}, \tag{3}$$

and the corresponding Hamiltonian (1) is thus called the Dicke-lattice model [52] (Rabi-lattice model for $N = 1$ [37–41], with N being the atom number of each site). Obviously, since the rotating-wave approximation is not employed, the TMDL model is able to completely describe potential effects arising from the counter-rotating terms and is therefore reasonable in the ultrastrong coupling regime, which has been achieved in current experiments of circuit QED [33–36].

The emergence of the so-called counter-rotating terms in the Dicke Hamiltonian (3) reduces the conservation of its excitation number, $\hat{N}_{s,j} = \hat{J}_{z,j} + \hat{a}_{1,j}^{\dagger}\hat{a}_{1,j}$, to a parity $\Pi = \exp(i\pi \hat{N}_{s,j})$. However, by introducing an extra degenerate photon mode $\hat{a}_{2,j}$, Hamiltonian (2) exhibits a special conserved excitation [53],

$$\hat{N}_{e,j} = \hat{J}_{z,j} + \hat{a}_{1,j}^{\dagger}\hat{a}_{2,j} + \hat{a}_{2,j}^{\dagger}\hat{a}_{1,j}, \tag{4}$$

apart from the known conserved parity [54], even if the rotating-wave approximation is not applied. When the photon hopping is triggered on, this conserved local excitation $\hat{N}_{e,j}$ is replaced by a global one,

$$\hat{N}_e = \sum_j \hat{N}_{e,j} = \sum_j (\hat{J}_{z,j} + \hat{a}_{1,j}^{\dagger}\hat{a}_{2,j} + \hat{a}_{2,j}^{\dagger}\hat{a}_{1,j}), \tag{5}$$

which manifests the U(1) symmetry of Hamiltonian (1). The conserved global excitation $\hat{N}_e$ and its induced U(1) symmetry distinguish the TMDL model from the standard single-mode Dicke-lattice model (with a discrete Z_2 symmetry and without conserved excitation). This complete change of symmetry is expected to deeply impact many-body physics of strongly correlated photons.

III. GROUND-STATE PHASE DIAGRAM

Since the knowledge of the single-site limit is crucial for further understanding many-body physics, before proceeding, we first catch some instructive insights into Hamiltonian (2). In the absence of photon hopping ($t = 0$), the excitation density commutes with Hamiltonian (1), i.e., $[\hat{N}_{e,j}, \hat{H}_{j}^{\mathrm{TD}}] = 0$, and each eigenstate is thus characterized by a certain excitation number. With an increasing system parameter, the level crossings of the lowest eigenstates are expected to take place, switching a definite excitation density of the ground state. Armed with this argument, we plot the ground-state mean excitation density, $n = \langle \hat{N}_{e,j} \rangle$, of the single-site Hamiltonian (2) as a function of g in Fig. 1. The evolution of n reflects a conspicuous staircase, whose jump points are associated with the crossover points of the lowest energy levels. For $N = 1$, n remains a constant, whereas with increasing N, the staircase appears and becomes more and more crowded, showing that the level crossing occurs only for $N \geqslant 2$. This property is remarkably different from the standard single-mode Dicke model (3), where no staircase can be found for any N (see the inset in Fig. 1), due to the nonconservation of its excitation

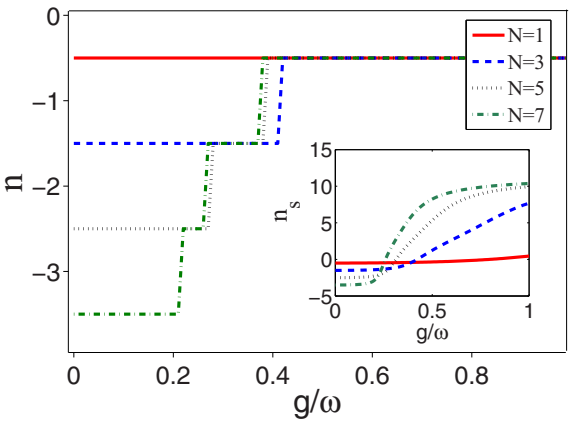

FIG. 1. The ground-state mean excitation densities, $n = \langle \hat{N}_{e,j} \rangle$, of the two-mode Dicke model (2) as functions of g/ω for different N. Inset: the mean excitation densities, $n_s = \langle \hat{N}_{s,j} \rangle$, of the standard Dicke model. In these figures, we set $\omega_0/\omega = 1$.

density $\hat{N}_{s,j}$. Additionally, notice that n takes negative and noninteger values, which is different from the known results in the Bose-Hubbard model with only positive integer fillings. This can be understood by investigating the definition of the excitation density operator $\hat{N}_{e,j}$, which can be rewritten as a more intuitive form, $\hat{N}_{e,j} = \hat{J}_{z,j} + \hat{b}^{\dagger}_{1,j}\hat{b}_{1,j} - \hat{b}^{\dagger}_{2,j}\hat{b}_{2,j}$, with respect to two new independent bosonic operators $\hat{b}_{1,j} = (\hat{a}_{1,j} + \hat{a}_{2,j})/\sqrt{2}$ and $\hat{b}_{2,j} = (\hat{a}_{1,j} - \hat{a}_{2,j})/\sqrt{2}$. The minus sign between $\hat{b}^{\dagger}_{1,j}\hat{b}_{1,j}$ and $\hat{b}^{\dagger}_{2,j}\hat{b}_{2,j}$, together with the appearance of the spin operator $\hat{J}_{z,j}$, distinguishes $\hat{N}_{e,j}$ from the conventional particle operator in the Bose-Hubbard model, and importantly, gives rise to the possibility of negative or noninteger values of n. It is therefore more convenient to visualize the lowest value of n, although negative, as zero particle filling and so on for n with higher values.

We now pay attention to the TMDL Hamiltonian (1). By applying a mean-field decoupling approximation [27], i.e., $\hat{a}^{\dagger}_{m,j}\hat{a}_{m,k} = \langle\hat{a}^{\dagger}_{m,j}\rangle\hat{a}_{m,k} + \langle\hat{a}_{m,k}\rangle\hat{a}^{\dagger}_{m,j} - \langle\hat{a}^{\dagger}_{m,j}\rangle\langle\hat{a}_{m,k}\rangle$, the many-body Hamiltonian (1) reduces to an effective mean-field Hamiltonian

$$\hat{H}_{\mathcal{MF}} = \sum_j \hat{H}^{\mathrm{TD}}_j - zt\sum_{j,m}[\psi_m(\hat{a}^{\dagger}_{m,j} + \hat{a}_{m,j}) - |\psi_m|^2], \qquad (6)$$

where z denotes the number of nearest neighbors, and $\psi_m = \langle\hat{a}_{m,j}\rangle$ $(m = 1,2)$ is the variational SF order parameter, which is taken to be real for simplicity [8,55]. ψ_m can be determined self-consistently by minimizing the ground-state energy $E(\psi_1,\psi_2)$ of the mean-field Hamiltonian (6) [8]. Notice that the explicit geometry of the lattice influences the mean-field result only through the coordination number z. A change of z amounts to a rescaling of the hopping rate t. For clarity, in the following analysis we assume $z = 3$, which could be, for example, a honeycomb lattice.

The effective mean-field Hamiltonian (6) reveals intimate connections between the single-site Hamiltonian (2) and the many-body properties. In general, even though the global excitation $\hat{N}_e$ is a conserved quantity, the excitation density $\hat{N}_{e,j}$ does not conserve, due to photon hopping. However, as shown in Hamiltonian (6), if both ψ_1 and ψ_2 vanish, the system dynamics is dominated by the single-site Hamiltonian (2), and the photons at each site are thus effectively frozen and characterized by a specific excitation number n. We accordingly denote this case as a MI phase, in which the U(1) symmetry is preserved. Whereas a U(1) symmetry-broken phase, associated with the breaking of the conservation of $\hat{N}_{e,j}$, is symbolized by a nonzero value of ψ_m and can be anticipated across a critical hopping rate $t_c(g)$. In this condition, the photon mode m governs a macroscopic coherence over the lattice and we have a SF phase of the mode m. It was generally believed that the complete inclusion of the counter-rotating terms would demolish the MI phase since they couple states with different numbers of the dressed photons and therefore inhibit the formation of photon blockade, which is crucially necessary for the MI phase [37–40]. In such a case, the notion "SF-MI" should be replaced by "coherent-incoherent". Nevertheless, the TMDL model we introduced here offers a superb exception: although still breaking the conventional conservation of $\hat{N}_{s,j}$, the counter-rotating terms in the TMDL model preserve the hybridized two-mode excitation $\hat{N}_{e,j}$, attributed to the special atom-photon coupling scheme in Hamiltonian (2), and thus retain the possibility to form the SF-MI quantum phase transition.

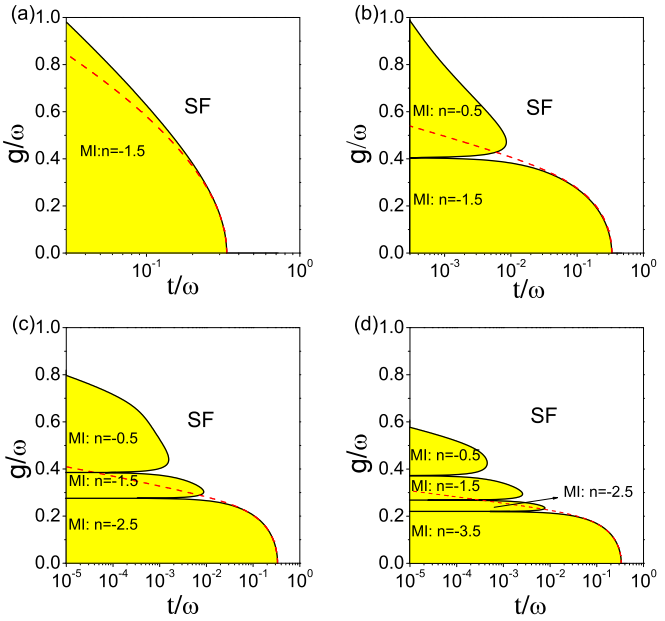

FIG. 2. Ground-state phase diagrams of Hamiltonian (6) in the $t-g$ plane with $z = 3$, when (a) $N = 1$, (b) $N = 3$, (c) $N = 5$, and (d) $N = 7$. The MI phase is characterized by its lobes, each of which supports a constant mean excitation density $n = \langle\hat{N}_{e,j}\rangle$. For a comparison, the phase boundaries of the Dicke-lattice model are also shown by the red dashed curves. In these figures, we set $\omega_0/\omega = 1$.

Based on above considerations, we plot the ground-state phase diagram in the t-g plane for different N in Fig. 2. These results show two typical phases: the U(1) symmetry-preserved MI with $\psi_1 = \psi_2 = 0$ and the symmetry-broken SF with nonzero ψ_1 and ψ_2. A further analysis of ψ_m near the critical point demonstrates that the transition between these two phases is of second order. According to Landau's theory [56,57], the phase boundary of this continuous transition can be obtained by a perturbation method, in which the ground-state energy $E_n(\psi_1,\psi_2)$ is expanded up to second order in ψ_m [14,39]. We expand $E_n(\psi_1,\psi_2)$ of the nth MI phase around the critical value of the order parameter $\psi_m = 0$. The expanded ground-state energy in powers of $zt\psi$ reads

$$E_n(\psi_1,\psi_2) = E^{(0)}_n + E^{(2)}_n + O(tz\psi)^4, \qquad (7)$$

where the second-order energy correction is

$$E^{(2)}_n = \sum_{m=1,2}(zt + z^2t^2R_{m,n})|\psi_m|^2 + 2z^2t^2T_n\psi_1\psi_2. \qquad (8)$$

The coefficients $R_{m,n}$ and T_n in Eq. (8) are derived from the second-order perturbation theory by

$$R_{m,n} = \sum_{k\neq n}\frac{|\langle n|(\hat{a}_{m,j} + \hat{a}^{\dagger}_{m,j})|k\rangle|^2}{E^{(0)}_n - E^{(0)}_k}, \qquad (9)$$

and

$$T_n = \sum_{k\neq n} \frac{[\langle n|(\hat{a}_{1,j} + \hat{a}^{\dagger}_{1,j})|k\rangle\langle k|(\hat{a}_{2,j} + \hat{a}^{\dagger}_{2,j})|n\rangle + \text{c.c}]}{2(E^{(0)}_n - E^{(0)}_k)}, \quad (10)$$

where $E^{(0)}_k$ and $|k\rangle$ arise from the eigenequation $\hat{H}^{\rm TD}_j|k\rangle = E^{(0)}_k|k\rangle$.

The critical hopping rate t_c can be obtained by the following procedure. (i) We first write a 2×2 Hessian matrix in terms of Eq. (8), i.e., $\mathcal{M}_{ij} = \partial^2 E^{(2)}_n/\partial\psi_i\partial\psi_j$, and then derive its two eigenvalues ε_1 and ε_2. (ii) These two eigenvalues generate two equations, $\varepsilon_1 = 0$ and $\varepsilon_2 = 0$, with respect to t. Each of these equations, say $\varepsilon_m = 0$, supports a trivial solution $t^T_m = 0$ and a nontrivial solution $t^N_m \neq 0$. (iii) The critical transition point is finally given by

$$t_c = \min\left(t^N_1, t^N_2\right). \quad (11)$$

The obtained boundaries are shown by the black solid curves in Fig. 2. The most important finding, as expected, is that the missing Mott lobes in the standard single-mode Dicke-lattice model [37,38] (see the red dashed curve in Fig. 2) reappear. More interestingly, our predicted Mott-lobe structure depends crucially on the atom number N, which has no counterpart in the Jaynes-Cummings-lattice [3–7] and Bose-Hubbard [27–31] models (Note that the N-dependent phase diagram for the Tavis-Cummings-lattice, which is nothing but the Dicke-lattice after the rotating-wave approximation, has been investigated previously [55,58,59]. In that case, the atom number N only slightly shifts the phase boundary of each lobe, rather than its total structure). Specifically, when $N = 1$, the atom-photon coupling features only a single Mott lobe, as shown in Fig. 2(a). With increasing N, however, more and more Mott lobes emerge, as shown in Figs. 2(b)–2(d). This N-dependent behavior of the Mott lobes is a direct legacy of the N-dependent staircase of n governed by the single-site Hamiltonian (2). In fact, since in the MI phase, the mean-field Hamiltonian (6) equals the single-site Hamiltonian (2), there exists a one-to-one correspondence between Figs. 1 and 2. As a result, each Mott lobe is specified by a definite mean excitation density n.

We emphasize that in the TMDL model, on the one hand, no chemical potential is needed to engineer the Mott lobes, which are here stabilized by the atom-photon coupling instead [38,39]. This is in sharp contrast to both cases of the Jaynes-Cummings-lattice [3–7] and Bose-Hubbard [27–31] models, which are often studied within the framework of a grand-canonical ensemble where a chemical potential is introduced to fix the (conserved) number of excitations on the lattice [8,14]. On the other hand, the standard single-mode Dicke- or Rabi-lattice model does not support any conserved excitations, due to the inclusion of the counter-rotating terms. This makes the description of the grand-canonical ensemble irrelevant to some extent and no well-defined chemical potential thus exists [56,57]. However, the conserved excitation in the TMDL model motivates us to introduce a chemical potential μ and access a theory of the grand-canonical ensemble. We now extend Eq. (1) to the following Hamiltonian in a grand-canonical ensemble:

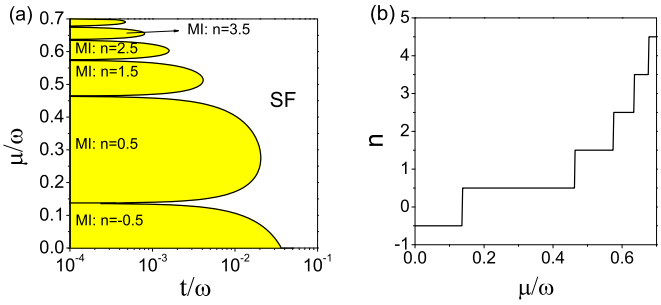

FIG. 3. (a) Ground-state phase diagram of Hamiltonian (12) in the t-μ plane with $z = 3$ and (b) the corresponding mean excitation density, $n = \langle\hat{N}_{e,j}\rangle$, of the single-site limit as a function of μ/ω. In these figures, we set $g/\omega = \omega_0/\omega = 1$ and $N = 1$.

$$\hat{H}_{\rm G} = \hat{H}_{\rm C} - \mu\hat{N}_e = \sum_j \hat{H}^{\rm GTD}_j - t\sum_{\langle j,k\rangle}\sum_{m=1,2}\hat{a}^{\dagger}_{m,j}\hat{a}_{m,k}, \quad (12)$$

where the on-site two-mode Dicke Hamiltonian becomes $\hat{H}^{\rm GTD}_j = \hat{H}^{\rm TD}_j - \mu\hat{N}_{e,j}$. Following the same mean-field theory, we plot the phase diagram in the t-μ plane in Fig. 3. As shown in Fig. 3(a), the engineered chemical potential μ still features the Mott lobes, which is a direct analog of those of the Bose-Hubbard model [27–31]. Once again, a clear interpretation of this lobe structure is still based on the dynamics of the single-site limit, which is governed by the Hamiltonian $\hat{H}^{\rm GTD}_j$. As the chemical potential couples to a conserved quantity $\hat{N}_{e,j}$ in the Hamiltonian $\hat{H}^{\rm GTD}_j$, the eigenstates are independent of μ, due to the simultaneous diagonalization of $\hat{H}^{\rm TD}_j$ and $\hat{N}_{e,j}$. Thus, the ground-state competition leads to a staircase behavior of the excitation density $\hat{N}_{e,j}$ when varying μ, as shown in Fig. 3(b). And accordingly, each Mott lobe in Fig. 3(a) is characterized by the corresponding plateaus.

IV. EFFECTIVE SPIN MODEL: CONTINUOUS XX MODEL

It has been well established that the Jaynes-Cummings-lattice model, respecting a U(1) symmetry, can be mapped to a continuous XX spin model (the isotropic XY spin model) [11,14], whereas the Rabi-lattice model with the counter-rotating terms has been demonstrated to be in the Ising universality class, owing to its discrete Z_2 symmetry [38,39,41]. As revealed in this paper, however, the inclusion of the counter-rotating terms does not always break the continuous symmetry. Especially, for our TMDL model, the U(1) symmetry associated with the conserved excitation number is a signature of its intimate connection with the continuous spin model. To confirm this argument, we focus on the system dynamics in the t-g plane, which is governed by Hamiltonian (1). We first consider the case of $N \geqslant 2$, which supports a multilobe structure in the phase diagram.

When parameters are tuned close to the degenerate point in the MI phase with $t \ll g$, i.e., the boundary between two nearest Mott lobes, we can truncate the Hilbert space to two of the excitation number eigenstates $|n\rangle$ and $|n+1\rangle$, where

$|n\rangle$ denotes the eigenstate of the excitation density $\hat{N}_{e,j}$ with eigenvalue n (as verified numerically below, n varies only by one across the degenerate point). Utilizing the commutation relations between the photon annihilation operator $\hat{a}_{m,j}$ and the excitation number $\hat{N}_{e,j}$, we can map $\hat{a}_{m,j}$ in the reduced Hilbert space $\{|n\rangle, |n+1\rangle\}$ into

$$\hat{a}_{1,j} \to \alpha \hat{\Sigma}_j^- + \beta \hat{\Sigma}_j^+, \quad \hat{a}_{2,j} \to \alpha \hat{\Sigma}_j^- - \beta \hat{\Sigma}_j^+, \tag{13}$$

where $\hat{\Sigma}_j^+ = |n\rangle\langle n+1|$ and $\hat{\Sigma}_j^- = |n+1\rangle\langle n|$ are the redefined Pauli spin ladder operators, and the coefficients α and β can be determined numerically (see Appendix A for details). Therefore, the effective spin Hamiltonian of the TMDL model reads

$$\hat{H} = \frac{\Delta}{2} \sum_i \hat{\Sigma}_i^z - J \sum_{\langle i,j \rangle} \left(\hat{\Sigma}_i^x \hat{\Sigma}_j^x + \hat{\Sigma}_i^y \hat{\Sigma}_j^y \right), \tag{14}$$

where Δ is the energy gap between the two states $|n\rangle$ and $|n+1\rangle$ and acts as a longitudinal field, and $J = 2t(|\alpha|^2 + |\beta|^2)$ is the isotropic exchange interaction. As expected, we reproduce the continuous XX spin model even though the counter-rotating terms are taken into account.

We now turn to the special case of $N = 1$, where only a single Mott lobe exists. In this case, the mapping procedure of $N \geqslant 2$ cannot be employed directly. However, similar to Ref. [38], the energy gap between the two lowest energy levels is of a higher-order small quantity, compared with the gap to the next energy level in the ultrastrong coupling regime, and the numerical calculation verifies that these two lowest levels are still characterized by the two nearest excitation numbers n and $n+1$ (see Appendix B). Based on these facts, in the ultrastrong coupling regime, we can still obtain the effective Hamiltonian (14) in the subspace spanned by the two lowest energy levels.

V. POSSIBLE EXPERIMENTAL IMPLEMENTATION

Having revealed some striking features of the two-mode cavity array, we now turn to the experimental implementation of Hamiltonian (1). Motivated by recent experimental achievements of cavity array [42–44] and multimode cavity [45–47] in circuit QED, we propose a scheme, depicted in Fig. 4, to implement the TMDL model. As shown in Fig. 4(a), the structure we consider is a series of identical circuit QED elements coupled through capacities. Each of these elements simulates the single-site two-mode Dicke model (2) and the capacitive coupling gives rise to the photon hopping of different elements (the schematic diagram of cavity array depicted here is a one-dimensional version for intuitive reasons, but this coupling scheme is essentially applicable to any other lattice geometries). The effective circuit diagram of each element is shown in Fig. 4(b). A Josephson junction, acting as an artificial two-level atom, is coupled to two different superconducting stripline resonators.

We first focus on the circuit QED element labeled in Fig. 4(a) with $N = 1$. According to the theory of circuit QED, we can regard the flux ϕ and the charge Q as the canonical coordinate and momentum, respectively. In this sense, the

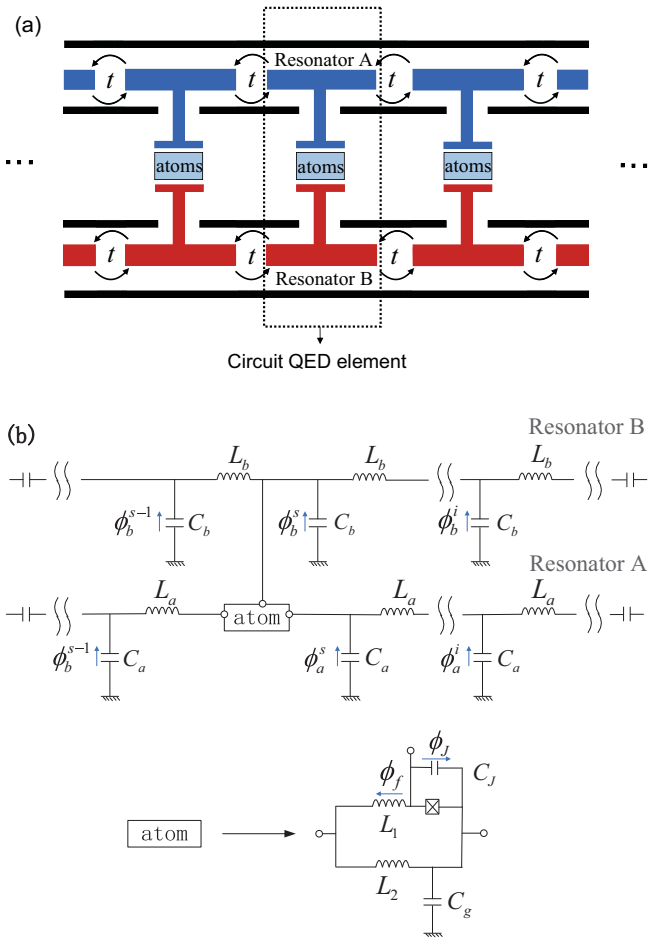

FIG. 4. (a) Schematic diagram of our proposed two-mode coupled circuit QED elements (black dashed line), one of which contains a couple of superconducting stripline resonators and finite Josephson junctions acting as artificial two-level atoms. The nearest two elements are coupled through the series capacitance of the resonators with a photon hopping rate t. (b) The effective circuit diagram of each element. The fabricated artificial atom (black dashed line) is assumed to be placed at a point, which is labeled by the superscript s of the flux.

Lagrangian of a circuit QED element in Fig. 4(b) is written as

$$\begin{aligned}\mathcal{L} = &\sum_i C_b \frac{(\dot{\phi}_b^i)^2}{2} + \sum_{i \neq s} \left[C_a \frac{(\dot{\phi}_a^i)^2}{2} + C_J \frac{(\dot{\phi}_J)^2}{2} \right. \\ &\left. + \tilde{C}_g \frac{(\dot{\phi}_b^s + \dot{\phi}_J)^2}{2} \right] - \sum_{i \neq s} \left[\frac{(\phi_a^{i-1} - \phi_a^i)^2}{2L_a} - \frac{(\phi_f)^2}{2L_1} \right. \\ &\left. - \frac{(\phi_f - \phi_J)^2}{2L_2} - \frac{(\phi_a^{s-1} - \phi_a^s - \phi_f + \phi_J)^2}{2L_a} \right] \\ &- \sum_i \frac{(\phi_b^{i-1} - \phi_b^i)^2}{2L_b} - E_J \cos\left(\frac{\phi_J + \phi_{\text{ext}}}{\phi_0} \right),\end{aligned} \tag{15}$$

where $\tilde{C}_g = C_g + C_a$ and ϕ_{ext} is the external flux of the Josephson junction. Notice that in deriving Eq. (15), the relation $\dot{\phi}_a^s = \dot{\phi}_b^s + \dot{\phi}_J$ has been used. Moreover, in terms of the Kirchoff's law at the point, there exists an extra constraint

relation $\phi_f = (L_1L_a + L_1L_2)\phi_J/L_\Sigma + L_1L_2(\phi_a^{s-1} - \phi_a^s)/L_\Sigma$, where $L_\Sigma = L_2L_a + L_1L_a + L_1L_2$.

Using $Q_k^j = \partial\mathcal{L}/\partial\dot{\phi}_k^j$, we obtain the expression of $\dot{\phi}_k^j$ in terms of Q_k^j, i.e.,

$$\begin{pmatrix}\dot{\phi}_J\\ \dot{\phi}_b^s\end{pmatrix} = \frac{1}{C_\Sigma}\begin{pmatrix}C_b + \tilde{C}_g, & -\tilde{C}_g\\ -\tilde{C}_g, & C_J + \tilde{C}_g\end{pmatrix}\begin{pmatrix}Q_J\\ Q_b^s\end{pmatrix} \tag{16}$$

and

$$\dot{\phi}_m^{i\neq s} = \frac{1}{C_m}Q_m^{i\neq s} \ (m = 1,2\,), \tag{17}$$

where $C_\Sigma = \tilde{C}_gC_b + \tilde{C}_gC_J + C_JC_b$.

By means of Eqs. (15)–(17), together with the relation between the Lagrangian and the Hamiltonian, we expand the Hamiltonian of the circuit QED element as a sum of three contributions, i.e.,

$$H_s = H_{res} + H_{at} + H_{int}. \tag{18}$$

In Eq. (18), the Hamiltonian of the stripline resonator is given by

$$\begin{aligned}H_{res} = \sum_i\Bigg[&\frac{\left(Q_b^i\right)^2}{2C_b} + \frac{\left(\phi_b^i - \phi_b^{i-1}\right)^2}{2L_b}\frac{\left(Q_a^i\right)^2}{2C_a} + \frac{\left(\phi_a^i - \phi_a^{i-1}\right)^2}{2L_a}\Bigg]\\ &+\left(\frac{\tilde{C}_g + C_J}{2C_\Sigma} - \frac{1}{2C_b}\right)\left(Q_b^s\right)^2 - \frac{\left(Q_a^s\right)^2}{2C_a}\\ &+\left(\frac{\tilde{L}_s}{2L_\Sigma^2L_2L_a} - \frac{1}{2L_a}\right)\left(\phi_a^s - \phi_a^{s-1}\right)^2.\end{aligned} \tag{19}$$

Since the last three terms in Hamiltonian (19) do not involve a sum over sites, their contributions can be neglected in the continuous limit, where the number of sites becomes infinite. Based on this consideration, we obtain

$$\begin{aligned}H_{res} = \sum_i\Bigg[&\frac{\left(Q_b^i\right)^2}{2C_b} + \frac{\left(\phi_b^i - \phi_b^{i-1}\right)^2}{2L_b} + \frac{\left(Q_a^i\right)^2}{2C_a}\\ &+\frac{\left(\phi_a^i - \phi_a^{i-1}\right)^2}{2L_a}\Bigg].\end{aligned} \tag{20}$$

The Hamiltonian of the artificial atom reads

$$\begin{aligned}H_{at} = &\frac{\tilde{C}_g + C_b}{2C_\Sigma}(Q_J)^2 + \frac{\tilde{L}_J}{2L_\Sigma^2L_2L_a}(\phi_J)^2\\ &- E_J\cos\left(\frac{\phi_J + \phi_{ext}}{\phi_0}\right).\end{aligned} \tag{21}$$

The interaction between the artificial atom and the resonator is governed by the Hamiltonian

$$H_{int} = \frac{\tilde{L}_c}{2L_\Sigma^2L_2L_a}\phi_J\left(\phi_a^s - \phi_a^{s-1}\right) - \frac{\tilde{C}_g}{C_\Sigma}Q_JQ_b^s. \tag{22}$$

In Eqs. (19)–(22), $\tilde{L}_J = L_1^2L_2^3 + 3L_1^2L_2^2L_a + 3L_1^2L_2L_a + 3L_1^2L_2L_a^2 + L_1^2L_a^3 + L_1L_2^3L_a + 2L_1L_2^2L_a^2 + L_1L_2L_a^3 - 2L_\Sigma L_1L_2^2 - 4L_\Sigma L_1L_2L_a - 2L_\Sigma L_1L_a^2 + L_\Sigma^2L_2 + L_\Sigma^2L_a$, $\tilde{L}_s = L_1^2L_2^3 + L_1^2L_2^2L_a + L_1L_2^3L_a - 2L_\Sigma L_1L_2^2 + L_\Sigma^2L_2$, and $\tilde{L}_c = 4L_\Sigma L_1L_2^2 + 4L_\Sigma L_1L_2L_a - 2L_1^2L_2^3 - 4L_1^2L_2^2L_a - 2L_1^2L_2L_a^2 - 2L_1L_2^3L_a - 2L_1L_2^2L_a^2 - 2L_\Sigma^2L_2$.

We thus take the continuous limit of the canonical parameters in the superconducting stripline resonators, i.e., $\phi_m^i \to \phi_m(x_i)$ and $Q_m^i \to Q_m(x_i)$, and then promote them to quantum operators obeying the canonical commutation relation $[\hat{\phi}_m(x), \hat{Q}_n(y)] = i\delta(x-y)\delta_{m,n}$. Following the standard quantization procedure in circuit QED [60], the quantized canonical parameters are expressed as

$$\begin{aligned}\hat{\phi}_m(x_i) = &\sum_{n_o=1}\frac{\sqrt{\omega_{m,n_o}L_mD}}{n_o\pi}\cos\left(\frac{n_o\pi x_i}{D}\right)\left(\hat{a}_{m,n_o} + \hat{a}_{m,n_o}^\dagger\right)\\ &+\sum_{n_e=2}\frac{\sqrt{\omega_{m,n_e}L_mD}}{n_e\pi}\sin\left(\frac{n_e\pi x_i}{D}\right)\left(\hat{a}_{m,n_e} + \hat{a}_{m,n_e}^\dagger\right),\end{aligned} \tag{23}$$

$$\begin{aligned}\hat{Q}_m(x_i) = &-i\sum_{n_o=1}\frac{\sqrt{\omega_{m,n_o}C_mD}}{n_o\pi}\cos\left(\frac{n_o\pi x_i}{D}\right)\left(\hat{a}_{m,n_o} - \hat{a}_{m,n_o}^\dagger\right)\\ &-i\sum_{n_e=2}\frac{\sqrt{\omega_{m,n_e}C_mD}}{n_e\pi}\sin\left(\frac{n_e\pi x_i}{D}\right)\left(\hat{a}_{m,n_e} - \hat{a}_{m,n_e}^\dagger\right),\end{aligned} \tag{24}$$

where $\omega_{m,n} = n\pi/(D\sqrt{L_mC_m})$ is the eigenfrequency, D is the length of the resonator, and n_o and n_e are odd and even integers, respectively.

When the external flux is set to $\phi_{ext}/\phi_0 = \pi$, the two-level approximation of the Josephson junction gives that [61,62]

$$\hat{\phi}_J \Leftrightarrow \langle\downarrow|\hat{\phi}_J|\uparrow\rangle\hat{\sigma}_x, \tag{25}$$

and

$$\hat{Q}_J \Leftrightarrow \frac{\omega_0}{4eE_Q\phi_0}\langle\downarrow|\hat{\phi}_J|\uparrow\rangle\hat{\sigma}_y, \tag{26}$$

with $E_Q = (\tilde{C}_g + C_b)/(2C_\Sigma)$, where ω_0 is the resonant frequency of the two-level system, $|\downarrow\rangle$ and $|\uparrow\rangle$ are the two lowest macroscopic states of the Hamiltonian H_{at}, and $\hat{\sigma}_i$ $(i = x,y,z)$ is the Pauli spin operator spanned by these two macroscopic states.

At low temperature, we only keep the mode resonant with the artificial atom (i.e., $n = 1$) and neglect other nonresonant terms. Under this single-mode approximation of the resonator and the two-level approximation of the artificial atom, the Hamiltonian of the considered circuit QED element is finally expressed as

$$\begin{aligned}\hat{H}_s = &\omega_1\hat{a}_1^\dagger\hat{a}_1 + \omega_2\hat{a}_2^\dagger\hat{a}_2 + \tfrac{1}{2}\omega_0\hat{\sigma}_z\\ &+g_1(\hat{a}_1 + \hat{a}_1^\dagger)\hat{\sigma}_x + ig_2(\hat{a}_2 - \hat{a}_2^\dagger)\hat{\sigma}_y,\end{aligned} \tag{27}$$

where

$$g_1 = -\frac{\tilde{L}_c\sqrt{\omega_1/L_aD}\sin(\pi x_s/D)\langle\downarrow|\hat{\phi}_J|\uparrow\rangle}{2L_\Sigma^2L_2}, \tag{28}$$

$$g_2 = \frac{\tilde{C}_g\omega_0\sqrt{\omega_2C_bD}\cos(\pi x_s/D)\langle\downarrow|\hat{\phi}_J|\uparrow\rangle}{4\pi eE_Q\phi_0C_\Sigma}, \tag{29}$$

$$\omega_1 = \frac{\pi}{D\sqrt{L_aC_a}}, \tag{30}$$

$$\omega_2 = \frac{\pi}{D\sqrt{L_bC_b}}. \tag{31}$$

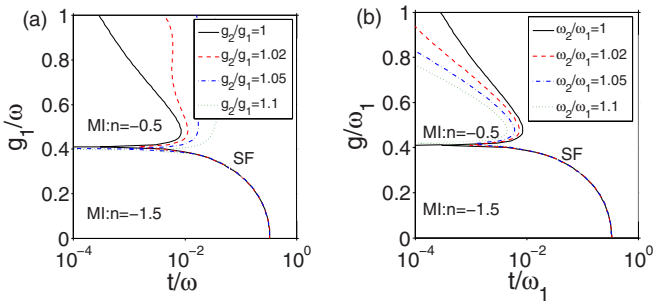

FIG. 5. (a) Phase boundaries for $g_2/g_1 = 1$, 1.02, 1.05, and 1.1, when $\omega_1/\omega = \omega_2/\omega = \omega_0/\omega = 1$. (b) Phase boundaries for $\omega_2/\omega_1 = 1$, 1.02, 1.05, and 1.1, when $g_1/g = g_2/g = \omega_0/\omega_1 = 1$. We set $N = 3$ and $z = 3$.

The tunability of the inductance and the capacitance of the two superconducting stripline resonators allows us to set $\omega_1 = \omega_2 = \omega$ and $g_1 = g_2 = g_0$, under which Hamiltonian (27) reduces to the single-site two-mode Rabi model. Using the same procedure, Hamiltonian (27) can be extended straightforwardly to the case with several two-level artificial atoms, i.e., the single-site two-mode Dicke Hamiltonian (2). When a series of such circuit QED elements are coupled capacitively with the hopping rate t [see Fig. 4(a)], the TMDL Hamiltonian (1) can be achieved.

We emphasize that the improvement of current experimental techniques in the ultrastrong coupling circuit QED [33–36] makes our proposal a promising candidate for exhibiting relevant physics of the TMDL model.

VI. DISCUSSIONS

Up to now, our discussions have been restricted to the cases of the degenerate photon modes ($\omega_1 = \omega_2 = \omega$) and the equal atom-photon coupling strengths ($g_1 = g_2 = g$). If these conditions are not fulfilled, there would not be a strict conservation law of $\hat{N}_e$, and an instructive question is whether the Mott-lobe structure still exists in such a case or not. To briefly show the influence of a slight deviation of these two equalities, $\omega_1 = \omega_2 = \omega$ and $g_1 = g_2 = g$, we plot the phase diagrams in the t-g plane for different ω_2/ω_1 [Fig. 5(b)] or g_2/g_1 [Fig. 5(a)], when $N = 3$. It can be seen clearly from these figures that a slight deviation of the ideal condition does not break the Mott-lobe structure but merely shifts the phase boundary.

VII. CONCLUSION

In summary, we have constructed a type of cavity array system, which is governed by the TMDL model. This model incorporates all of the counter-rotating terms of the atom-photon coupling and therefore works well in the ultrastrong coupling regime achieved in recent experiments. Unlike the standard single-mode Dicke-lattice model, the TMDL has a global conserved excitation and a continuous U(1) symmetry. This distinct change of symmetry via adding an extra photon mode strongly impacts the nature of photon localization and delocalization behavior. Specifically, the atom-photon interaction features Mott-lobe structures of photons and a second-order SF-MI quantum phase transition, which share similarities with the Jaynes-Cummings-lattice and Bose-Hubbard models. However, the Mott-lobe structures predicted here depend crucially on the atom number of each site, reflecting its particularity among lattice models. We have also shown that the TMDL model can be mapped into a continuous XX spin model under proper parameter conditions. Finally, we have proposed an experimentally feasible scheme to realize the TMDL model in a two-mode superconducting stripline cavity array.

ACKNOWLEDGMENTS

This work is supported partly by the NSFC under Grants No. 11422433, No. 11674200, No. 11604392, No. 11434007, and No. 61378049; the PCSIRT under Grant No. IRT13076; the FANEDD under Grant No. 201316; SFSSSP; OYTPSP; and SSCC.

APPENDIX A: MAPPING $\hat{a}_{1,j}$ AND $\hat{a}_{2,j}$ TO THE SPIN OPERATORS

We first notice that the commutation relations between the photon annihilation operator and the excitation number operator satisfy

$$[\hat{a}_{1,j}, \hat{N}_{e,j}] = \hat{a}_{2,j}, \quad [\hat{a}_{2,j}, \hat{N}_{e,j}] = \hat{a}_{1,j}. \tag{A1}$$

Taking these two equations into account, the matrix elements of $\hat{a}_{1,j} + \hat{a}_{2,j}$ and $\hat{a}_{1,j} - \hat{a}_{2,j}$ in the basis of the excitation eigenstates $|n\rangle$ and $|m\rangle$ are expressed respectively as

$$\begin{aligned} \langle n|\hat{a}_{1,j} + \hat{a}_{2,j}|m\rangle &= \langle n|[\hat{a}_{1,j} + \hat{a}_{2,j}, \hat{N}_{e,j}]|m\rangle \\ &= (m-n)\langle n|\hat{a}_{1,j} + \hat{a}_{2,j}|m\rangle, \end{aligned} \tag{A2}$$

$$\begin{aligned} \langle n|a_{1,j} - a_{2,j}|m\rangle &= -\langle n|[\hat{a}_{1,j} - \hat{a}_{2,j}, N_{e,j}]|m\rangle \\ &= (n-m)\langle n|\hat{a}_{1,j} - \hat{a}_{2,j}|m\rangle. \end{aligned} \tag{A3}$$

To obtain a nonzero value of $\langle n|\hat{a}_{1,j} + \hat{a}_{2,j}|m\rangle$ ($\langle n|\hat{a}_{1,j} - \hat{a}_{2,j}|m\rangle$), we should have $m = n + 1$ ($m = n - 1$), and in the reduced Hilbert space $\{|n\rangle, |n+1\rangle\}$, the operators $\hat{a}_{1,j} + \hat{a}_{2,j}$

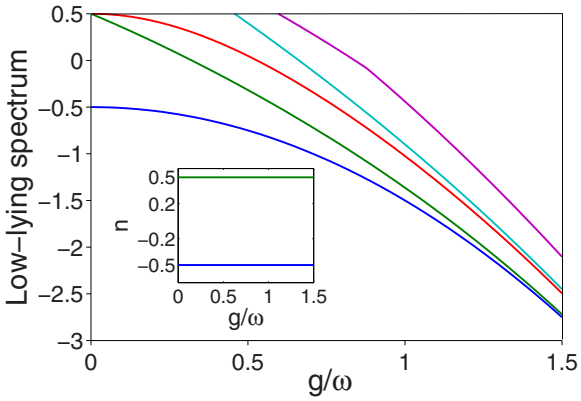

FIG. 6. Low-lying spectrum of Hamiltonian (2) (in units of ω) as a function of g/ω. Inset: the excitation numbers n of the two lowest levels. We set $\omega_0/\omega = 1$ and $N = 1$.

and $\hat{a}_{1,j} - \hat{a}_{2,j}$ thus read

$$\hat{a}_{1,j} + \hat{a}_{2,j} \to 2\alpha \begin{pmatrix} 0 & 0 \\ 1 & 0 \end{pmatrix} \Leftrightarrow 2\alpha \hat{\Sigma}_j^-, \tag{A4}$$

$$\hat{a}_{1,j} - \hat{a}_{2,j} \to 2\beta \begin{pmatrix} 0 & 1 \\ 0 & 0 \end{pmatrix} \Leftrightarrow 2\beta \hat{\Sigma}_j^+, \tag{A5}$$

from which we can straightforwardly obtain $\hat{a}_{1,j} \to \alpha \hat{\Sigma}_j^- + \beta \hat{\Sigma}_j^+$ and $a_{2,j} \to \alpha \hat{\Sigma}_j^- - \beta \hat{\Sigma}_j^+$, i.e., Eq. (13) of the main text. The coefficients α and β can be determined numerically.

APPENDIX B: NUMERICAL DEMONSTRATION OF THE TWO-STATE SUBSPACE $\{|n\rangle, |n+1\rangle\}$ IN THE ULTRASTRONG COUPLING REGIME FOR $N = 1$

Figure 6 shows the low-lying spectrum of Hamiltonian (2) with $N = 1$, from which we can see clearly that the two lowest energy levels become quasidegenerate in the ultrastrong coupling regime. Moreover, as shown in the inset of this figure, both of these levels support the well-defined excitation numbers, whose difference remains one. This guarantees the validity of the truncation of the Hilbert space to an effective two-state subspace $\{|n\rangle, |n+1\rangle\}$ for a large g/ω.

[1] T. E. Northup and R. Blatt, Quantum information transfer using photons, Nat. Photon. **8**, 356 (2014).

[2] I. Carusotto and C. Ciuti, Quantum fluids of light, Rev. Mod. Phys. **85**, 299 (2013).

[3] M. J. Hartmann, F. G. S. L. Brandão, and M. B. Plenio, Quantum many-body phenomena in coupled cavity arrays, Laser Photon. Rev. **2**, 527 (2008).

[4] A. A. Houck, H. E. Türeci, and J. Koch, On-chip quantum simulation with superconducting circuits, Nat. Phys. **8**, 292 (2012).

[5] S. Schmidt and J. Koch, Circuit QED lattices: Towards quantum simulation with superconducting circuits, Ann. Phys. (Berlin) **525**, 395 (2013).

[6] I. M. Georgescu, S. Ashhab, and F. Nori, Quantum simulation, Rev. Mod. Phys. **86**, 153 (2014).

[7] C. Noh and D. G. Angelakis, Quantum simulations and many-body physics with light, Rep. Prog. Phys. **80**, 016401 (2017).

[8] A. D. Greentree, C. Tahan, J. H. Cole, and L. C. L. Hollenberg, Quantum phase transition of light, Nat. Phys. **2**, 856 (2006).

[9] M. J. Hartmann, F. G. S. L. Brandão, and M. B. Plenio, Strongly interacting polaritons in coupled arrays of cavities, Nat. Phys. **2**, 849 (2006).

[10] M. J. Hartmann, F. G. S. L. Brandão, and M. B. Plenio, Effective Spin Systems in Coupled Microcavities, Phys. Rev. Lett. **99**, 160501 (2007).

[11] D. G. Angelakis, M. F. Santos, and S. Bose, Photon-blockade-induced Mott transitions and XY spin models in coupled cavity arrays, Phys. Rev. A **76**, 031805(R) (2007).

[12] M. I. Makin, J. H. Cole, C. Tahan, L. C. L. Hollenberg, and A. D. Greentree, Quantum phase transitions in photonic cavities with two-level systems, Phys. Rev. A **77**, 053819 (2008).

[13] S. Schmidt and G. Blatter, Strong Coupling Theory for the Jaynes-Cummings-Hubbard Model, Phys. Rev. Lett. **103**, 086403 (2009).

[14] J. Koch and K. L. Hur, Superfluid–Mott-insulator transition of light in the Jaynes-Cummings lattice, Phys. Rev. A **80**, 023811 (2009).

[15] K. Toyoda, Y. Matsuno, A. Noguchi, S. Haze, and S. Urabe, Experimental Realization of a Quantum Phase Transition of Polaritonic Excitations, Phys. Rev. Lett. **111**, 160501 (2013).

[16] G. Kulaitis, F. Krüger, F. Nissen, and J. Keeling, Disordered driven coupled cavity arrays: Nonequilibrium stochastic mean-field theory, Phys. Rev. A **87**, 013840 (2013).

[17] K. Kamide, M. Yamaguchi, T. Kimura, and T. Ogawa, First-order superfluid–Mott-insulator transition for quantum-optical switching in cavity-QED arrays with two cavity modes, Phys. Rev. A **87**, 053842 (2013).

[18] S. Felicetti, G. Romero, D. Rossini, R. Fazio, and E. Solano, Photon transfer in ultrastrongly coupled three-cavity arrays, Phys. Rev. A **89**, 013853 (2014).

[19] B. Bujnowski, J. K. Corso, A. L. C. Hayward, J. H. Cole, and A. M. Martin, Supersolid phases of light in extended Jaynes-Cummings-Hubbard systems, Phys. Rev. A **90**, 043801 (2014).

[20] M. Biondi, E. P. L. van Nieuwenburg, G. Blatter, S. D. Huber, and S. Schmidt, Incompressible Polaritons in a Flat Band, Phys. Rev. Lett. **115**, 143601 (2015).

[21] Y. Zhang, J. Fan, J.-Q. Liang, J. Ma, G. Chen, S. Jia, and F. Nori, Photon devil's staircase: Photon long-range repulsive interaction in lattices of coupled resonators with Rydberg atoms, Sci. Rep. **5**, 11510 (2015).

[22] K. Seo and L. Tian, Quantum phase transition in a multiconnected superconducting Jaynes-Cummings lattice, Phys. Rev. B **91**, 195439 (2015).

[23] M. Schiró, C. Joshi, M. Bordyuh, R. Fazio, J. Keeling, and H. E. Türeci, Exotic Attractors of the Nonequilibrium Rabi-Hubbard Model, Phys. Rev. Lett. **116**, 143603 (2016).

[24] M.-J. Hwang and M. B. Plenio, Quantum Phase Transition in the Finite Jaynes-Cummings Lattice Systems, Phys. Rev. Lett. **117**, 123602 (2016).

[25] A. Maggitti, M. Radonjić, and B. M. Jelenković, Dark-polariton bound pairs in the modified Jaynes-Cummings-Hubbard model, Phys. Rev. A **93**, 013835 (2016).

[26] A. L. C. Hayward and A. M. Martin, Superfluid-Mott transitions and vortices in the Jaynes-Cummings-Hubbard lattices with time-reversal-symmetry breaking, Phys. Rev. A **93**, 023828 (2016).

[27] M. P. A. Fisher, P. B. Weichman, G. Grinstein, and D. S. Fisher, Boson localization and the superfluid-insulator transition, Phys. Rev. B **40**, 546 (1989).

[28] D. van Oosten, P. van der Straten, and H. T. C. Stoof, Quantum phases in an optical lattice, Phys. Rev. A **63**, 053601 (2001).

[29] J. K. Freericks and H. Monien, Phase diagram of the Bose-Hubbard model, Europhys. Lett. **26**, 545 (1994).

[30] J. K. Freericks and H. Monien, Strong-coupling expansions for the pure and disordered Bose-Hubbard model, Phys. Rev. B **53**, 2691 (1996).

[31] T. D. Küner and H. Monien, Phases of the one-dimensional Bose-Hubbard model, Phys. Rev. B **58**, R14741 (1998).
[32] I. Bloch, J. Dalibard, and W. Zwerger, Many-body physics with ultracold gases, Rev. Mod. Phys. **80**, 885 (2008).
[33] T. Niemczyk, F. Deppe, H. Huebl, E. P. Menzel, F. Hocke, M. J. Schwarz, J. J. García-Ripoll, D. Zueco, T. Hümmer, E. Solano, A. Marx, and R. Gross, Circuit quantum electrodynamics in the ultrastrong-coupling regime, Nat. Phys. **6**, 772 (2010).
[34] P. Forn-Díaz, J. Lisenfeld, D. Marcos, J. J. García-Ripoll, E. Solano, C. J. P. M. Harmans, and J. E. Mooij, Observation of the Bloch-Siegert Shift in a Qubit-Oscillator System in the Ultrastrong Coupling Regime, Phys. Rev. Lett. **105**, 237001 (2010).
[35] P. Forn-Díaz, J. J. García-Ripoll, B. Peropadre, J.-L. Orgiazzi, M. A. Yurtalan, R. Belyansky, C. M. Wilson, and A. Lupascu, Ultrastrong coupling of a single artificial atom to an electromagnetic continuum in the nonperturbative regime, Nat. Phys. **13**, 39 (2017).
[36] F. Yoshihara, T. Fuse, S. Ashhab, K. Kakuyanagi, S. Saito, and K. Semba, Superconducting qubit–oscillator circuit beyond the ultrastrong-coupling regime, Nat. Phys. **13**, 44 (2017).
[37] H. Zheng and Y. Takada, Importance of counter-rotating coupling in the superfluid-to-Mott-insulator quantum phase transition of light in the Jaynes-Cummings lattice, Phys. Rev. A **84**, 043819 (2011).
[38] M. Schiró, M. Bordyuh, B. Öztop, and H. E. Tü reci, Phase Transition of Light in Cavity QED Lattices, Phys. Rev. Lett. **109**, 053601 (2012).
[39] M. Schiró, M. Bordyuh, B. Öztop, and H. E. Türeci, Quantum phase transition of light in the Rabi-Hubbard model, J. Phys. B **46**, 224021 (2013).
[40] T. Flottat, F. Hébert, V. G. Rousseau, and G. G. Batrouni, Quantum Monte Carlo study of the Rabi-Hubbard model, Eur. Phys. J. D **70**, 213 (2016).
[41] B. Kumar and S. Jalal, Quantum Ising dynamics and Majorana-like edge modes in the Rabi lattice model, Phys. Rev. A **88**, 011802(R) (2013).
[42] J. Raftery, D. Sadri, S. Schmidt, H. E. Türeci, and A. A. Houck, Observation of a Dissipation-Induced Classical to Quantum Transition, Phys. Rev. X **4**, 031043 (2014).
[43] C. Eichler, Y. Salathe, J. Mlynek, S. Schmidt, and A. Wallraff, Quantum-Limited Amplification and Entanglement in Coupled Nonlinear Resonators, Phys. Rev. Lett. **113**, 110502 (2014).
[44] M. Fitzpatrick, N. Sundaresan, A. C. Y. Li, J. Koch, and A. A. Houck, Observation of a Dissipative Phase Transition in a One-Dimensional Circuit QED Lattice, Phys. Rev. X **7**, 011016 (2017).
[45] M. Mariantoni, H. Wang, R. C. Bialczak, M. Lenander, E. Lucero, M. Neeley, A. D. O'Connell, D. Sank, M. Weides, J. Wenner, T. Yamamoto, Y. Yin, J. Zhao, J. M. Martinis, and A. N. Cleland, Photon shell game in three-resonator circuit quantum electrodynamics, Nat. Phys. **7**, 287 (2011).
[46] N. M. Sundaresan, Y. Liu, D. Sadri, László J. Szőcs, D. L. Underwood, M. Malekakhlagh, H. E. Türeci, and A. A. Houck, Beyond Strong Coupling in a Multimode Cavity, Phys. Rev. X **5**, 021035 (2015).
[47] D. C. McKay, R. Naik, P. Reinhold, L. S. Bishop, and D. I. Schuster, High-Contrast Qubit Interactions Using Multimode Cavity QED, Phys. Rev. Lett. **114**, 080501 (2015).
[48] R. Englman, *The Jahn-Tellwe Effect in Molecules and Crystals* (Wiley, New York, 1972).
[49] J. Larson, Jahn-Teller systems from a cavity QED perspective, Phys. Rev. A **78**, 033833 (2008).
[50] J. Larson, Analog of the spin-orbit-induced anomalous Hall effect with quantized radiation, Phys. Rev. A **81**, 051803(R) (2010).
[51] D. Porras, P. A. Ivanov, and F. Schmidt-Kaler, Quantum Simulation of the Cooperative John-Teller Transition in 1D Ion Crystals, Phys. Rev. Lett. **108**, 235701 (2012).
[52] L. J. Zou, D. Marcos, S. Diehl, S. Putz, J. Schmiedmayer, J. Majer, and P. Rabl, Implementation of the Dicke Lattice Model in Hybrid Quantum System Arrays, Phys. Rev. Lett. **113**, 023603 (2014).
[53] J. Fan, Z. Yang, Y. Zhang, J. Ma, G. Chen, and S. Jia, Hidden continuous symmetry and Nambu-Goldstone mode in a two-mode Dicke model, Phys. Rev. A **89**, 023812 (2014).
[54] C. Emary and T. Brandes, Chaos and the quantum phase transition in the Dicke model, Phys. Rev. E **67**, 066203 (2003).
[55] S.-C. Lei and R.-K. Lee, Quantum phase transition of light in the Dicke-Bose-Hubbard model, Phys. Rev. A **77**, 033827 (2008).
[56] J. P. Sethna, *Statistical Mechanics: Entropy, Order Parameters, and Complexity* (Oxford University Press, Oxford, 2006).
[57] K. Huang, *Statistical Mechanics* (Wiley, New York, 1987).
[58] D. Rossini and R. Fazio, Mott-Insulating and Glassy Phases of Polaritons in 1D Arrays of Coupled Cavities, Phys. Rev. Lett. **99**, 186401 (2007).
[59] M. Knap, E. Arrigoni, and W. von der Linden, Quantum phase transition and excitations of the Tavis-Cummings lattice model, Phys. Rev. B **82**, 045126 (2010).
[60] A. Blais, R.-S. Huang, A. Wallraff, S. M. Girvin, and R. J. Schoelkopf, Cavity quantum electrodynamics for superconducting electrical circuits: An architecture for quantum computation, Phys. Rev. A **69**, 062320 (2004).
[61] P. Nataf and C. Ciuti, Vacuum Degeneracy of a Circuit QED System in the Ultrastrong Coupling Regime, Phys. Rev. Lett. **104**, 023601 (2010).
[62] A. Baksic and C. Ciuti, Controlling Discrete and Continuous Symmetries in "Superradiant" Phase Transitions with Circuit QED Systems, Phys. Rev. Lett. **112**, 173601 (2014).